Rotor-Flux-Oriented Control of a Single-Phase Induction Motor Drive

Maurício Beltrão de Rossiter Corrêa, Cursino Brandão Jacobina, *Senior Member, IEEE*, Antonio Marcus Nogueira Lima, *Member, IEEE*, and Edison Roberto Cabral da Silva, *Senior Member, IEEE*

***Abstract*—This paper investigates the vector control of a single-phase induction motor drive to implement low-cost systems for low-power applications. The static power converter side is implemented using a single-phase rectifier cascaded with a four-switch inverter. The vector control is based upon field orientation concepts that have been adapted for this type of machine. Simulation and experimental results are provided to illustrate the system operation.**

***Index Terms*—Field-oriented control, single-phase induction motor.**

I. Introduction

SINGLE-PHASE machines are widely used for fractional- and subfractional-horsepower applications, although, for example, units of up to 12 hp can be found in rural applications. In general, the single-phase machine has both main and auxiliary windings, which usually have different impedances, and a squirrel-cage rotor. Among the single-phase motors that have two windings, the most common types are the split-phase, capacitor-start, capacitor-run, and capacitor-start capacitor-run. Only the split-phase motor does not use an auxiliary capacitor, and when the auxiliary capacitor (startup capacitor) needs to be cut out, this is done by a centrifugal switch.

The availability of low-cost static converters makes possible the economic use of energy and improvement of the quality of the electromagnetic torque in single-phase induction motor drives [1]–[6].

This paper investigates the use of the scheme in Fig. 1 for feeding a single-phase motor. The converter employed consists of a single-phase rectifier in series with a four-switch inverter (FSI) as was proposed in [7] and employed in [2] for a single-phase induction motor drive. This paper employs the same converter, but it investigates the use of the rotor-flux vector control in more detail, as well as the design of current and voltage digital controllers for a single-phase motor drive. Note that the scheme employed declines the use of capacitors, which are removed when they exist in the motor.

Feeding of both main and auxiliary windings allows the single-phase machine to be treated as a two-phase machine. However, the use of field orientation to control an unbalanced single-phase machine requires special attention because the mathematical model for this type of machine is similar to that of an asymmetrical two-phase machine. The approach presented here can be applied to any single-phase machine that has two windings. However, emphasis is given for the case in which the main and auxiliary windings have different impedances. Therefore, the proposed approach is recommended for applications in which it is required an improvement of the overall performance of a standard single-phase drive system when some physical or economical constraint impose keeping the existing machine.

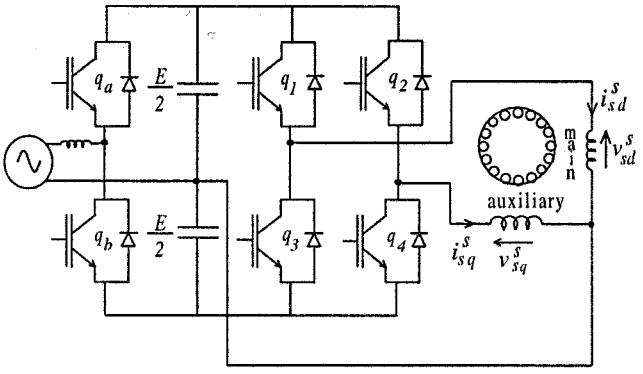

Fig. 1. Single-phase induction motor drive system.

The proposed configuration provides bidirectional power flow and power-factor control. The input and output converters can be implemented with a single six-switch device package in which one of the legs is used to implement the rectifier and the other two to implement the inverter. The computing power required to implement the techniques proposed fits quite well for a general purpose microcontroller. The use of a reduced number of power switches and a microcontroller while keeping the existing single-phase motor results in a low-cost drive system.

Simulation and experimental results are presented to demonstrate the main characteristics of the proposed drive system and to validate the methodology and the modeling approach employed in this work.

II. Machine Model

The equations that define the dynamic model for the single-phase induction machine are

$$v^s_{sd} = r_{sd} i^s_{sd} + \frac{d\phi^s_{sd}}{dt} \tag{1}$$

$$v^s_{sq} = r_{sq} i^s_{sq} + \frac{d\phi^s_{sq}}{dt} \tag{2}$$

Manuscript received May 30, 1999; revised March 12, 2000. Abstract published on the Internet April 21, 2000.

The authors are with the Laboratório de Eletrônica Industrial e Acionamento de Máquinas, Departamento de Engenharia Elétrica, Universidade Federal da Paraíba, 58109-970 Campina Grande, Brazil (e-mail: jacobina@dee.ufpb.br).

Publisher Item Identifier S 0278-0046(00)06825-8.

0278–0046/00$10.00 © 2000 IEEE

$$0 = r_r i^s_{rd} + \frac{d\phi^s_{rd}}{dt} + \omega_r \phi^s_{rq} \tag{3}$$

$$0 = r_r i^s_{rq} + \frac{d\phi^s_{rq}}{dt} - \omega_r \phi^s_{rd} \tag{4}$$

$$\phi^s_{sd} = l_{sd} i^s_{sd} + m_{srd} i^s_{rd} \tag{5}$$

$$\phi^s_{sq} = l_{sq} i^s_{sq} + m_{srq} i^s_{rq} \tag{6}$$

$$\phi^s_{rd} = l_r i^s_{rd} + m_{srd} i^s_{sd} \tag{7}$$

$$\phi^s_{rq} = l_r i^s_{rq} + m_{srq} i^s_{sq} \tag{8}$$

$$T_e = P(m_{srq} i^s_{sq} i^s_{rd} - m_{srd} i^s_{sd} i^s_{rq}) \tag{9}$$

$$P(T_e - T_m) = J\frac{d\omega_r}{dt} + F\omega_r \tag{10}$$

where v^s_{sd}, v^s_{sq}, i^s_{sd}, i^s_{sq}, i^s_{rd}, i^s_{rq}, ϕ^s_{sd}, ϕ^s_{sq}, ϕ^s_{rd} and ϕ^s_{rq} are the dq-axes voltages, currents, and fluxes of the stator and rotor in the stator reference frame (superscript s), r_{sd}, r_{sq} and r_r denote the stator and rotor resistances, l_{sd}, l_{sq}, l_r, m_{srd} and m_{srq} denote the stator, and the rotor self- and mutual inductances, ω_r, T_e and $T_m$are the machine speed, and the electromagnetic and the load torque, and P, J and F are the machine pole pairs, the inertia, and viscous friction coefficient.

This model was obtained using an approach similar to that used to obtain the dq model for an unbalanced two-phase machine. It is written in the stator reference frame to eliminate the terms that depend on the mechanical angle position [8].

III. Rotor-Flux Model

Due to the asymmetry of the stator main and auxiliary windings of the single-phase motor, the use of field-orientation principles requires a special attention, unlike the symmetrical machine, there is no standard definition of the vector model in the case of an asymmetrical machine. The asymmetry is a result of different d- and q-axes parameters, which is very common with standard single-phase machines. This asymmetry causes an oscillating term in the electromagnetic torque. Even when i^s_{sd} and i^s_{sq} have equal amplitudes and are phase shifted by 90°, an ac term in the torque still exists. This can be observed in the torque equation (9), where different values of mutual inductances are present, but, as will be demonstrated, it is possible to eliminate the electromagnetic torque ac term by means of an appropriate control of the stator currents.

The mathematical expression of the electromagnetic torque written in terms of the machine parameters and rotor fluxes can be derived from (7)–(9) and is given by

$$T_e = \frac{P}{l_r}\left(m_{srq} i^s_{sq} \phi^s_{rd} - m_{srd} i^s_{sd} \phi^s_{rq}\right). \tag{11}$$

Assuming that the stator currents can be imposed as

$$i^s_{sd} = i^s_{sd1} \tag{12}$$

$$i^s_{sq} = k i^s_{sq1} \tag{13}$$

with $k = m_{srd}/m_{srq}$, then by substituting the variables i^s_{sd} and i^s_{sq} for the auxiliary variables i^s_{sd1} and i^s_{sq1} into (11), the torque can be expressed by

$$T_e = \frac{P}{l_r} m_{srd}\left(i^s_{sq1} \phi^s_{rd} - i^s_{sd1} \phi^s_{rq}\right). \tag{14}$$

This expression is equivalent to that of the symmetric machine in which the oscillating term does not exist in steady state. Employing the current compensation given by (12) and (13), a vector model can also be developed to define the control strategy.

From (3), (4), (7), and (8) it is possible to derive dynamic equations, which relate rotor fluxes to rotor currents, as

$$\frac{d\phi^s_{rd}}{dt} = -\frac{1}{\tau_r}\phi^s_{rd} - \omega_r \phi^s_{rq} + \frac{1}{\tau_r} m_{srd} i^s_{sd} \tag{15}$$

$$\frac{d\phi^s_{rq}}{dt} = \omega_r \phi^s_{rd} - \frac{1}{\tau_r}\phi^s_{rq} + \frac{1}{\tau_r} m_{srq} i^s_{sq} \tag{16}$$

where $\tau_r = l_r/r_r$.

This model is not symmetric ($m_{srd} \neq m_{srq}$) and is, therefore, not suitable. However, by using (12) and (13), (15) and (16) can be written as

$$\frac{d\phi^s_{rd}}{dt} = -\frac{1}{\tau_r}\phi^s_{rd} - \omega_r \phi^s_{rq} + \frac{1}{\tau_r} m_{srd} i^s_{sd1} \tag{17}$$

$$\frac{d\phi^s_{rq}}{dt} = \omega_r \phi^s_{rd} - \frac{1}{\tau_r}\phi^s_{rq} + \frac{1}{\tau_r} m_{srd} i^s_{sq1}. \tag{18}$$

Now, a vector model can be defined. From (17) and (18), the rotor-flux model written for an arbitrary reference frame, denoted by the superscript a, is given by

$$\frac{d\boldsymbol{\phi}^a_r}{dt} = -\frac{1}{\tau_r}\boldsymbol{\phi}^a_r - j(\omega_a - \omega_r)\boldsymbol{\phi}^a_r + \frac{1}{\tau_r} m_{srd} \mathbf{i}^a_{s1} \tag{19}$$

where

$$\boldsymbol{\phi}^a_r = \phi^a_{rd} + j\phi^a_{rq} = \left(\phi^s_{rd} + j\phi^s_{rq}\right) e^{-j\delta_a}$$
$$\mathbf{i}^a_{s1} = i^a_{sd1} + j i^a_{sq1} = \left(i^s_{sd1} + j i^s_{sq1}\right) e^{-j\delta_a}$$

and $\omega_a = d\delta_a/dt$ and δ_a are the speed and the position of the arbitrary reference frame viewed from the stator, respectively.

The electromagnetic torque can be derived from (14), that is,

$$T_e = \frac{P}{l_r} m_{srd}\left(i^a_{sq1}\phi^a_{rd} - i^a_{sd1}\phi^a_{rq}\right). \tag{20}$$

IV. Rotor-Flux-Oriented Control

Based on the rotor-flux model derived previously, it is possible to use the field-orientation principles for decoupling the control of the flux and torque as presented in the following.

Equation (19), written in the rotor-flux reference frame (superscript e), can be decomposed into two equations

$$\frac{m_{srd}}{\tau_r} i^e_{sd1} = \frac{\phi_r}{\tau_r} + \frac{d\phi_r}{dt} \tag{21}$$

$$\frac{m_{srd}}{\tau_r} i^e_{sq1} = \omega_{sl}\phi_r \tag{22}$$

where ϕ_r is the rotor-flux amplitude, $\omega_{sl} = \omega_e - \omega_r$ is the slip frequency, and $\omega_e = d\delta_e/dt$ and δ_e are the frequency and the position of the rotor-flux vector viewed from the stator, respectively.

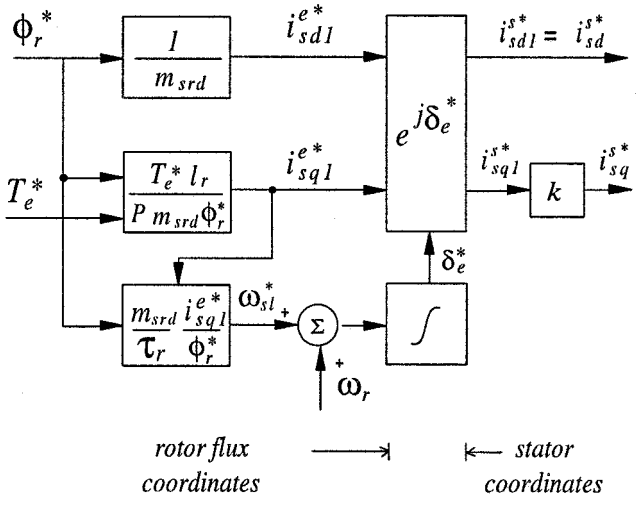

Fig. 2. Block diagram of the proposed field-oriented controller.

The expression for the torque in terms of the q-axis current and the rotor-flux amplitude can be derived from (20)

$$T_e = P\frac{m_{srd}}{l_r}\phi_r i^e_{sq1}. \tag{23}$$

From these results, it is possible to adopt the indirect field-oriented control scheme, as illustrated in Fig. 2, where T_e^* and ϕ_r^* represent the reference torque and the reference flux, respectively. The block $e^{j\delta_e^*}$ performs signal transformations from the synchronous frame to the stator frame. Furthermore, i_{sd}^{s*} and i_{sq}^{s*} represent the reference currents to be supplied to the machine.

V. Current Control

The rotor-flux control strategy presented here requires an internal loop for current control. The models employed for designing the stationary current controllers are obtained from (1)–(8) and are given by

$$v^s_{sd} = \left(r_{sd} + \frac{m^2_{srd}}{\tau_r l_r}\right) i^s_{sd} + \sigma_{sd} l_{sd}\frac{di^s_{sd}}{dt} + e^s_{sd} \tag{24}$$

$$v^s_{sq} = \left(r_{sq} + \frac{m^2_{srq}}{\tau_r l_r}\right) i^s_{sq} + \sigma_{sq} l_{sq}\frac{di^s_{sq}}{dt} + e^s_{sq} \tag{25}$$

where $\sigma_{sd} = 1 - m^2_{srd}/(l_r l_{sd})$ and $\sigma_{sq} = 1 - m^2_{srq}/(l_r l_{sq})$. The terms e^s_{sd} and e^s_{sq} are the counter electromotive forces and are given by

$$e^s_{sd} = -\frac{m_{srd}}{l_r}\left(\omega_r \phi^s_{rq} + \frac{\phi^s_{rd}}{\tau_r}\right)$$

$$e^s_{sq} = \frac{m_{srq}}{l_r}\left(\omega_r \phi^s_{rd} - \frac{\phi^s_{rq}}{\tau_r}\right).$$

To implement the stator current control in synchronous coordinates, a suitable model must be obtained. To derive such a model, it is necessary to find a compensation factor for the dq voltage components, as has been done for the current components [see (12) and (13)]. An approximate voltage-compensating factor can be found by analyzing (24) and (25). At high speed, e^s_{sd} and e^s_{sq} dominate the other terms in the voltage equations and then $\mathcal{A}(v^s_{sd})/\mathcal{A}(v^s_{sq}) \cong m_{srd}/m_{srq} = k$. The term $\mathcal{A}(x)$ represents an operator that extracts the amplitude of the sinusoidal waveform x. Thus, the compensated components of the voltage and counter electromotive forces can be defined as $v^s_{sd1} = v^s_{sd}$, $v^s_{sq1} = kv^s_{sq}$, $e^s_{sd1} = e^s_{sd}$ and $e^s_{sq1} = ke^s_{sq}$. Introducing these compensated voltage components in (24) and (25), the following dq model can be written for an arbitrary reference frame:

$$v^a_{sd1} = \left(r_{sd} + \frac{m^2_{srd}}{\tau_r l_r}\right) i^a_{sd1} + \sigma_{sd} l_{sd}\frac{di^a_{sd1}}{dt} + e^a_{sd1} + \vartheta^a_{sd1} \tag{26}$$

$$v^a_{sq1} = \left(r_{sd} + \frac{m^2_{srd}}{\tau_r l_r}\right) i^a_{sq1} + \sigma_{sd} l_{sd}\frac{di^a_{sq1}}{dt} + e^a_{sq1} + \vartheta^a_{sq1} \tag{27}$$

where

$$\begin{aligned}
&v^a_{sd1} + jv^a_{sq1} \\
&\quad = \left(v^s_{sd1} + jv^s_{sq1}\right) e^{-j\delta_a} \\
&e^a_{sd1} + je^a_{sq1} \\
&\quad = \left[e^s_{sd1} + je^s_{sq1} + j\omega_a \sigma_{sd} l_{sd}\left(i^s_{sd1} + ji^s_{sq1}\right)\right] e^{-j\delta_a} \\
&\vartheta^a_{sd1} + j\vartheta^a_{sq1} \\
&\quad = j\left[\left(k^2 r_{sq} - r_{sd}\right) i^s_{sq1} + \left(k^2 l_{sq} - l_{sd}\right)\frac{di^s_{sq1}}{dt}\right] e^{-j\delta_a}.
\end{aligned}$$

The model given by (26) and (27) is almost symmetric when the machine unbalancing is only due to the difference in the number of turns of the main and auxiliary windings. In this case, $k^2 = m^2_{srd}/m^2_{srq} = l_{sd}/l_{sq}$ and, consequently, $k^2 l_{sq} - l_{sd} = 0$. Then, except in the low-speed range where $(k^2 r_{sq} - r_{sd}) i^s_{sq1}$ is more important, the residual voltages due to unbalancing represented by ϑ^a_{sd1} and ϑ^a_{sq1} are very small.

The simplest way to implement the current control loop is to use standard hysteresis controllers, as shown in Fig. 3(a), and which are particularly suitable for analog implementation.

In this paper, the current control loop implemented by using discrete-time proportional plus integral (PI) controllers is investigated in detail. Due to the machine asymmetry, the easiest solution is to implement the controller in stator coordinates. Implementing PI controllers in stator coordinates can be done as shown in Fig. 3(b), which is meant to complement Fig. 2. In this diagram, blocks R^s_d and R^s_q represent the PI controllers and block PWM+FSI+IM represent the pulsewidth modulator, inverter, and motor.

The synchronous controller in rotor-flux vector coordinates is based on (26) and (27) by making $\delta_a = \delta_e$ and replacing the superscript a by e in the variables. In this case, the expressions for the counter electromotive forces are

$$e^e_{sd1} = -m_{srd}\phi_r/(l_r\tau_r) - \omega_e \sigma_{sd} l_{sd} i^e_{sq1}$$

and

$$e^e_{sq1} = m_{srd}\omega_r \phi_r / l_r + \omega_e \sigma_{sd} l_{sd} i^e_{sd1}.$$

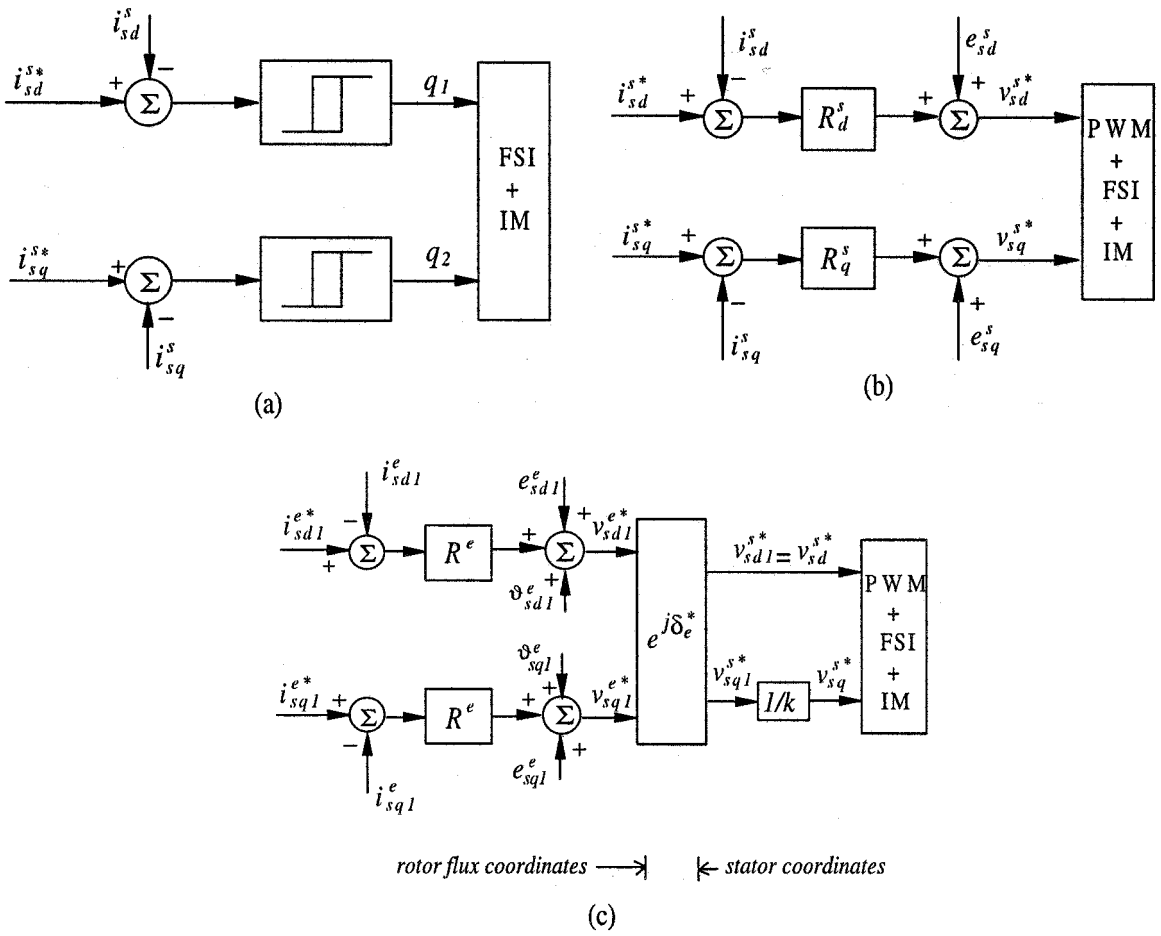

Fig. 3. Current controller block diagrams. (a) Hysteresis. (b) Stationary. (c) Synchronous.

The current control diagram is shown in Fig. 3(c). In this diagram, blocks R^e represent the PI controllers, the references i^{e*}_{sd1}, i^{e*}_{sq1} and δ^*_e are obtained from the diagram in Fig. 2, and

$$i^e_{sd1} = i^s_{sd1}\cos(\delta^*_e) + i^s_{sq1}\sin(\delta^*_e)$$

and

$$i^e_{sq1} = -i^s_{sd1}\sin(\delta^*_e) + i^s_{sq1}\cos(\delta^*_e).$$

The continuous-time PI controllers are designed to compensate the time constants

$$\sigma_{sd} l_{sd} \Big/ \left(r_{sd} + \frac{m^2_{srd}}{\tau_r l_r} \right)$$

and

$$\sigma_{sq} l_{sq} \Big/ \left(r_{sq} + \frac{m^2_{srq}}{\tau_r l_r} \right)$$

for the stationary controllers, and

$$\sigma_{sd} l_{sd} \Big/ \left(r_{sd} + \frac{m^2_{srd}}{\tau_r l_r} \right)$$

for the synchronous controllers, and also to provide the closed-loop performance according to the optimum damping criteria [9], [10]. The discrete-time controllers were obtained from the continuous-time controllers using Tustin approximation.

In this paper, the counter electromotive forces and the residual voltages due to unbalancing are considered as disturbances. In this case, the voltage decoupling [10] is achieved in a feedforward way at the output of the current controllers, as presented in Fig. 3(b) and (c). The influence of the disturbances compensation is discussed in Section VII.

VI. Inverter Pulsewidth Modulation (PWM) Control

The current control strategy presented in the previous section needs the machine voltage control, which is obtained here by using a modified space-vector PWM technique. Assume that the conduction state of the power switches in the inverter of Fig. 1 is associated to the binary variables q_1 to q_4; binary "1" indicates a closed switch and binary "0" an open switch. The pairs q_1–q_3 and q_2–q_4 are complementary and, as a consequence, $q_3 = 1$–q_1 and $q_4 = 1$–q_2.

Using the two-phase machine with the converter in Fig. 1, the dq voltages are given by

$$v^s_{sd} = \left(q_1 \frac{E}{2} - q_3 \frac{E}{2} \right) = (2q_1 - 1)\frac{E}{2} \tag{28}$$

$$v^s_{sq} = \left(q_2 \frac{E}{2} - q_4 \frac{E}{2} \right) = (2q_2 - 1)\frac{E}{2}. \tag{29}$$

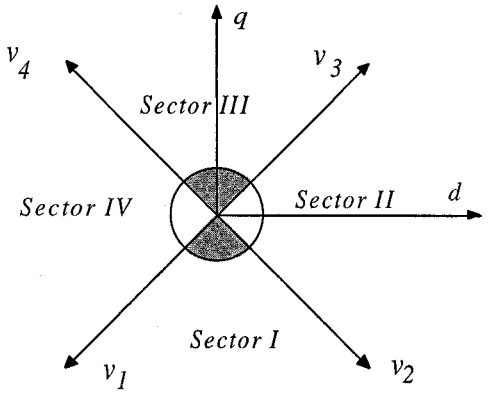

Fig. 4. Voltage vectors in the dq plane.

TABLE I
SECTORS GROUPING BY THE SIGN OF t_{13}

Sectors	Vectors	Condition
I,IV	$\mathbf{v_4v_1v_2}$	$t_{13} > 0$
II,III	$\mathbf{v_2v_3v_4}$	$t_{13} < 0$

TABLE II
SECTORS GROUPING BY THE SIGN OF t_{24}

Sectors	Vectors	Condition
I,II	$\mathbf{v_1v_2v_3}$	$t_{24} > 0$
III,IV	$\mathbf{v_1v_4v_3}$	$t_{24} < 0$

The combination of the states of the switches originates four different vectors in the plane dq

$$[q_1 = 0,\, q_2 = 0] \rightarrow \boldsymbol{v}_1 = \frac{E}{\sqrt{2}} e^{-j3\pi/4} = -(1+j)\frac{E}{2}$$
$$[q_1 = 1,\, q_2 = 0] \rightarrow \boldsymbol{v}_2 = \frac{E}{\sqrt{2}} e^{-j\pi/4} = (1-j)\frac{E}{2}$$
$$[q_1 = 1,\, q_2 = 1] \rightarrow \boldsymbol{v}_3 = \frac{E}{\sqrt{2}} e^{j\pi/4} = (1+j)\frac{E}{2}$$
$$[q_1 = 0,\, q_2 = 1] \rightarrow \boldsymbol{v}_4 = \frac{E}{\sqrt{2}} e^{j3\pi/4} = (-1+j)\frac{E}{2}. \quad (30)$$

Vectors of same amplitude are phase shifted by $\pi/2$ from each other. Using the above vector definitions, one may divide the dq plane into four (I–IV) sectors, as shown in Fig. 4.

Let $\boldsymbol{v}_s^*$ ($\boldsymbol{v}_s^* = v_{sd}^{s*} + jv_{sq}^{s*}$) represent the reference voltage to be synthesized by the inverter within one cycle time of length T. According to the space-vector technique

$$\boldsymbol{v}_s^* T = \boldsymbol{v}_1 t_1 + \boldsymbol{v}_2 t_2 + \boldsymbol{v}_3 t_3 + \boldsymbol{v}_4 t_4 \quad (31)$$

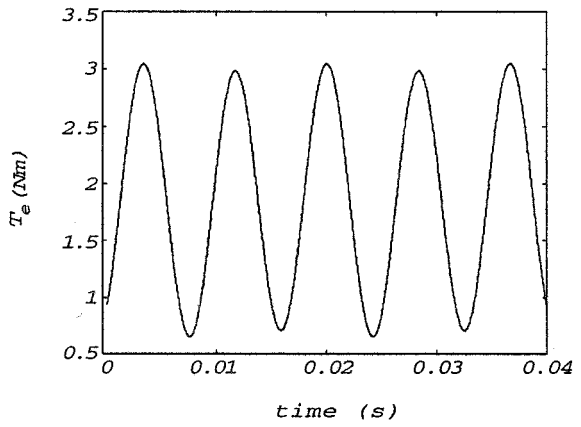

(a)

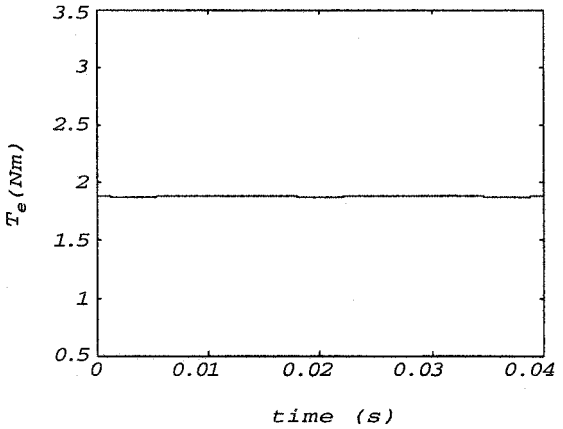

(b)

Fig. 5. Electromagnetic torque of the machine for (a) balanced voltages and (b) for compensated currents.

with the time weights t_1, t_2, t_3, and t_4 restricted to

$$T = t_1 + t_2 + t_3 + t_4. \quad (32)$$

The problem is how to find the values of the time weights given by $\boldsymbol{v}_s^*$ and T. In order to simplify the algebraic manipulation, introduce $\boldsymbol{v}_x = \boldsymbol{v}_1 = -\boldsymbol{v}_3 = -E/2 - jE/2$ and $\boldsymbol{v}_y = \boldsymbol{v}_2 = -\boldsymbol{v}_4 = E/2 - jE/2$. Replacing the vectors $\boldsymbol{v}_x$ and $\boldsymbol{v}_y$ into (31) results in

$$\boldsymbol{v}_s^* T = \boldsymbol{v}_x t_{13} + \boldsymbol{v}_y t_{24} \quad (33)$$

with $t_{13} = t_1 - t_3$ and $t_{24} = t_2 - t_4$.

From (31), one determines t_{13} and t_{24} as follows:

$$t_{13} = -\frac{T}{E}\left(v_{sd}^{s*} + v_{sq}^{s*}\right) \quad (34)$$
$$t_{24} = \frac{T}{E}\left(v_{sd}^{s*} - v_{sq}^{s*}\right). \quad (35)$$

Computation of the values of the time weights is an undetermined problem. To overcome this, assume that only three of the four vectors will be employed. In this case, one of the four time

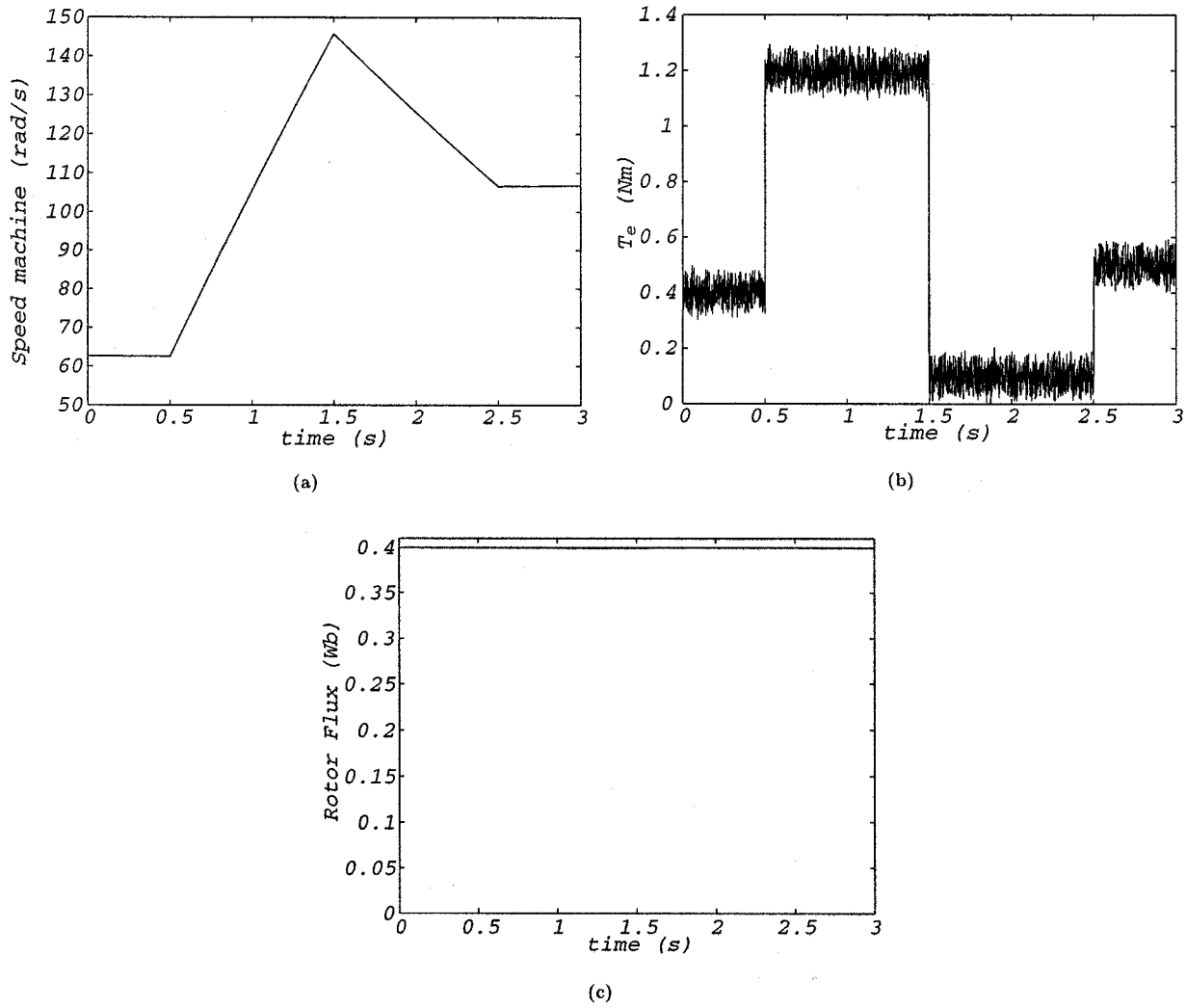

Fig. 6. (a) Machine speed, (b) electromagnetic torque, and (c) rotor flux for the proposed field-oriented control.

weights must be set equal to zero, which serves to not only solve the undetermined problem, but reduce the switching frequency of the inverter as well.

For each one of the sectors of Fig. 4 there exist two groups of three vectors that can be employed to compose the reference voltage, as shown in Tables I and II. As the vectors have the same amplitude, the utilization of Tables I and II produces similar effects. Using the test conditions given in Tables I or II and equations (32), (34), and (35) one may compute time weights t_1, t_2, t_3, and t_4.

One should observe that, due to the asymmetry between the stator windings, balanced operation of the single-phase machine requires different modulation indexes per phase.

VII. Simulation Results

Flux, torque, and current control were investigated with the help of a simulation program.

The effect of the current compensation may be observed by comparing the results obtained by feeding the machine with two different sources: 1) voltage source, $v_{sd}^s = V_s \cos\omega_e t$, $v_{sq}^s = V_s \sin\omega_e t$ and 2) current source with compensation, $i_{sd}^s = I_s \cos\omega_e t$, $i_{sq}^s = kI_s \sin\omega_e t$.

In Fig. 5, the torque waveforms for these two ideal sources are presented. It can be seen that the current compensation allows a continuous (nonoscillating) steady-state torque [Fig. 5(b)], compared to the voltage-source excitation where torque ripple is produced [Fig. 5(a)].

The simulation results obtained with the proposed field-oriented control strategy, using current sources obtained by hysteresis controllers, are shown in Fig. 6; here, the reference flux is kept constant at 0.4 Wb, while the reference torque is submitted to the step changes

$$\begin{aligned} T_e^* &= 0.4\ \text{N}\cdot\text{m}, && \text{for } 0 \le t < 0.5\ \text{s} \\ T_e^* &= 1.2\ \text{N}\cdot\text{m}, && \text{for } 0.5\text{s} \le t < 1.5\ \text{s} \\ T_e^* &= 0.1\ \text{N}\cdot\text{m}, && \text{for } 1.5\ \text{s} \le t < 2.5\ \text{s} \\ T_e^* &= 0.5\ \text{N}\cdot\text{m}, && \text{for } \le t \le 3.0\ \text{s}. \end{aligned}$$

It can be seen that the flux and torque control are fairly appropriate.

Fig. 7 illustrates the influence of counter electromotive forces in the performance of the current controller in four different sit-

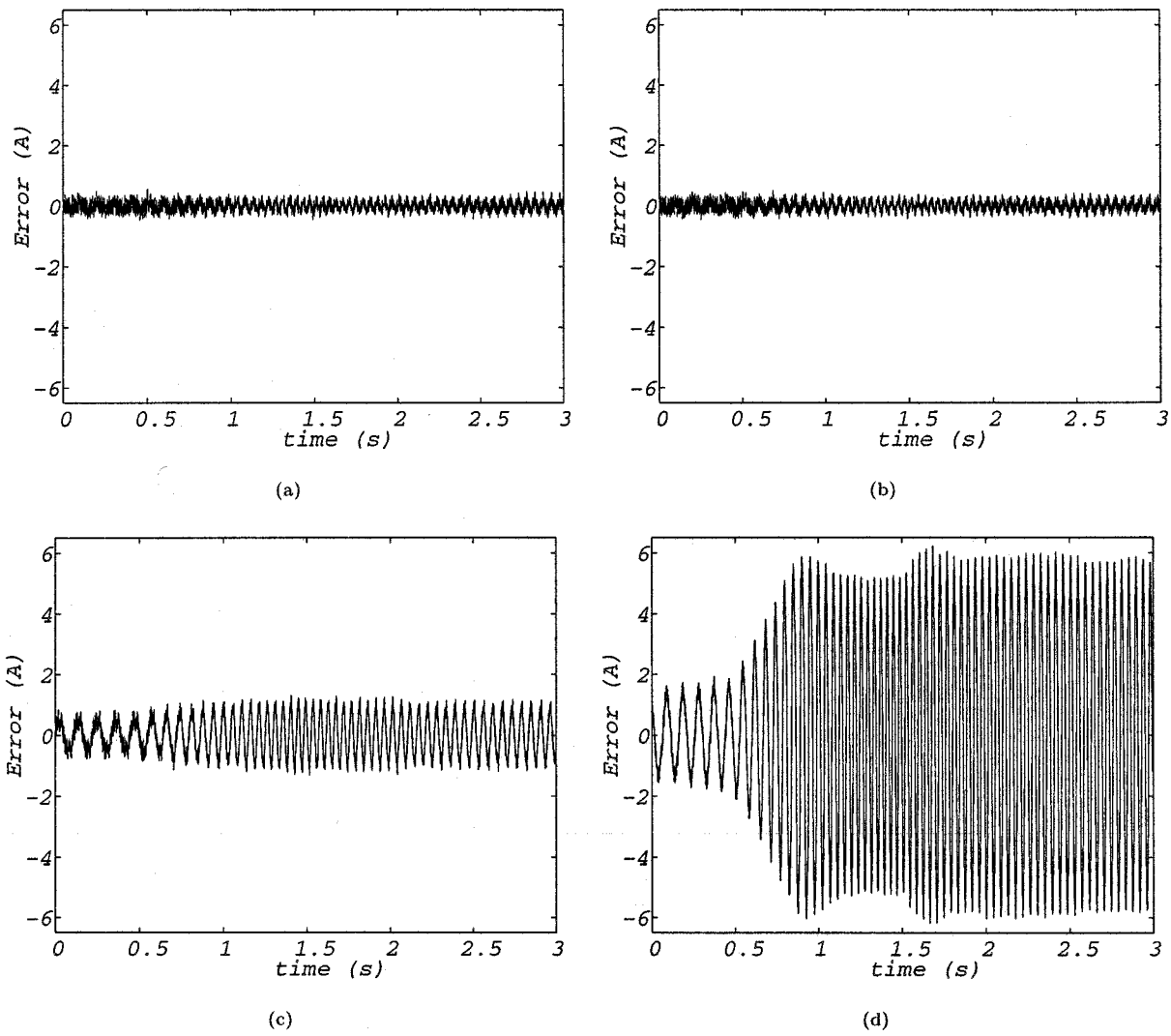

Fig. 7. q-axis current errors obtained for the synchronous and stationary controllers with and without compensation. (a) Synchronous with compensation. (b) Synchronous without compensation. (c) Stationary with compensation. (d) Stationary without compensation.

uations with two different control schemes. The control schemes are presented in Fig. 3(b) and (c) and have been used to implement the field-oriented strategy. In all four cases, the reference profiles used for the rotor-flux and electromagnetic torque are the same as used to obtain the waveforms of Fig. 6. Fig. 7(a) and (b) presents the current error for the q axis (i^{s*}_{sq}–i^{s}_{sq}) obtained with the current controller implemented in the synchronous reference frame with [Fig. 7(a)] and without [Fig. 7(b)] compensating for the electromotive forces e^{e}_{sd1} and e^{e}_{sq1}. Fig. 7(c) and (d) presents the current error for the q axis obtained with the current controller implemented in the stationary reference frame with [Fig. 7(c)] and without [Fig. 7(d)] compensating for the electromotive forces e^{s}_{sd} and e^{s}_{sq}. The q-axis current errors in Fig. 7(a) and (b) are less than 3% of the amplitude of the reference current. However, the errors observed in Fig. 7(c) and (d) reach up to 9% and 50%, respectively. From these results, we can conclude that compensating for the electromotive forces e^{s}_{sd} and e^{s}_{sq} has a pronounced impact in the improvement of the stationary controller performance. However, the improvement obtained by compensating for e^{e}_{sd1} and e^{e}_{sq1} in the synchronous controller was not so impressive. Moreover, the performance obtained with the stationary controller with compensation is worse than that obtained with the synchronous controller with or without compensation. Although results for the d-axis current error are not presented, the same conclusions are obtained by observing the waveforms for the current error in the d axis. Good performance of the current control loop in synchronous coordinates, without compensating for e^{e}_{sd1} and e^{e}_{sq1}, is expected because, in this case, the disturbances are continuous quantities and, consequently, the integrating term of the PI controller can cancel their effects. The effect of compensating for the residual voltages due to unbalancing is negligible, although not shown in this paper.

VIII. Experimental Results

The laboratory implementation of the control strategies discussed previously was carried out with the scheme sketched in Fig. 1. The drive system is composed of a static power converter, a 0.5-hp single-phase induction machine and a microcomputer (*PC-Pentium*). The generation of the command signals for the converter, data acquisition, and the control law tasks

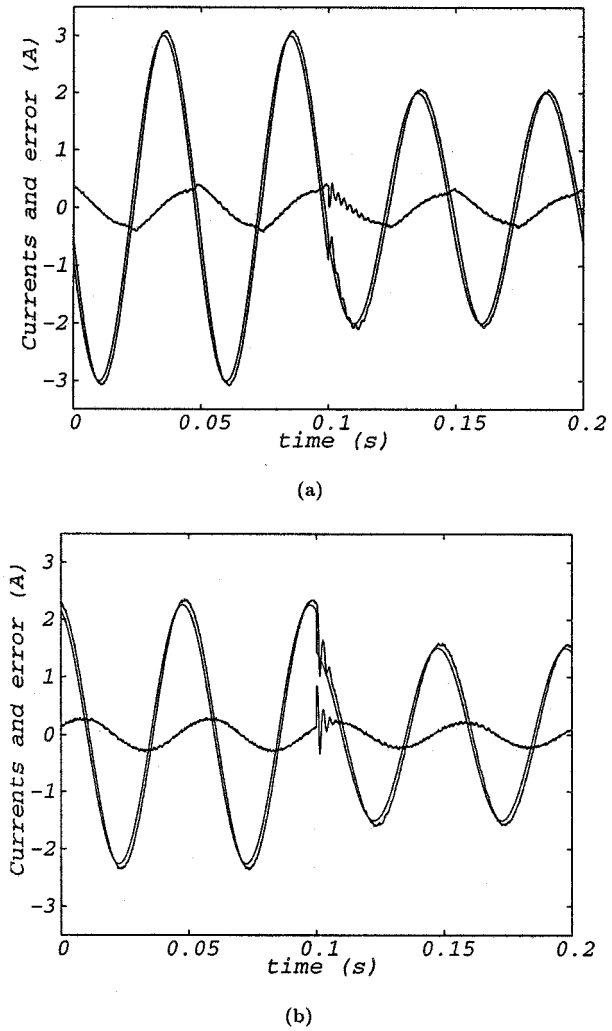

Fig. 8. Stator currents and current errors for the stationary controller at 20 Hz. (a) d axis. (b) q axis.

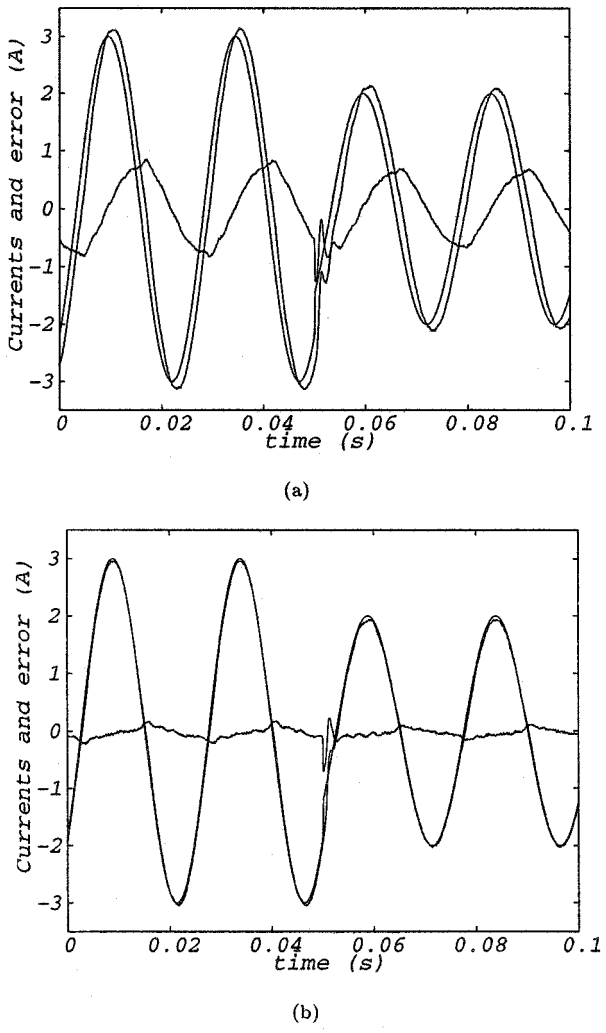

Fig. 9. Stator currents and current errors of d axis for the controllers at 40 Hz. (a) Stationary. (b) Synchronous.

are implemented around the microcomputer-based platform that is equipped with appropriate plug-in boards and sensors. The angular speed is obtained from the absolute position encoder that has a 9-b resolution. The stator currents are filtered by a second-order anti-aliasing filter and sampled at each 100 μs, i.e., $h = 100$ μs. The asymmetry constant k for the single-phase induction machine is 0.75. The generation of the PWM patterns was obtained using the technique presented in Section VI.

Figs. 8–10 present the actual (i^s_{sd}, i^s_{sq}) and reference (i^{s*}_{sd}, i^{s*}_{sq}) stator currents, which are superimposed, as well as their respective errors ($i^{s*}_{sd} - i^s_{sd}$, i^{s*}_{sq}–i^s_{sq}) obtained with the current controllers of Fig. 3(b) and (c) for three different values of stator frequency f_e, i.e., 20, 40, and 60 Hz. Only the controllers without compensation were considered. The reference currents are given by

$$\begin{aligned} i^{s*}_{sd} &= 3\cos(2\pi f^*_e t) \\ i^{s*}_{sq} &= 2.25\sin(2\pi f^*_e t), \qquad \text{for } 0 \le t < t_{\max}/2 \\ i^{s*}_{sd} &= 2\cos(2\pi f^*_e t) \\ i^{s*}_{sq} &= 1.5\sin(2\pi f^*_e t), \qquad \text{for } t_{\max}/2 \le t \le t_{\max} \end{aligned}$$

where $t_{\max}$ is the total time of the experimental test and the current amplitude is in amperes.

Fig. 8(a) and (b) presents the actual and reference stator currents and their respective errors, with the current controllers of Fig. 3(b) at 20 Hz. One should observe that the controllers present a maximum steady-state error of 22%. The results for the controller implemented with synchronous coordinates are not presented here, but they have been shown to have a maximum steady-state error less than 4%.

Fig. 9(a) and (b) shows the actual stator currents and their respective errors for the main phase, d, with the stationary controllers and synchronous controllers at 40 Hz. One should observe that the maximum current error for the synchronous controllers is smaller than that obtained with the stationary controllers.

Fig. 10(a) and (b) shows similar test results at 60 Hz, but only for the synchronous controllers. The maximum current error increases with respect to those observed in Fig. 9(b), but remains within acceptable margins (<8%). The stationary controllers present a maximum current error greater than 80%.

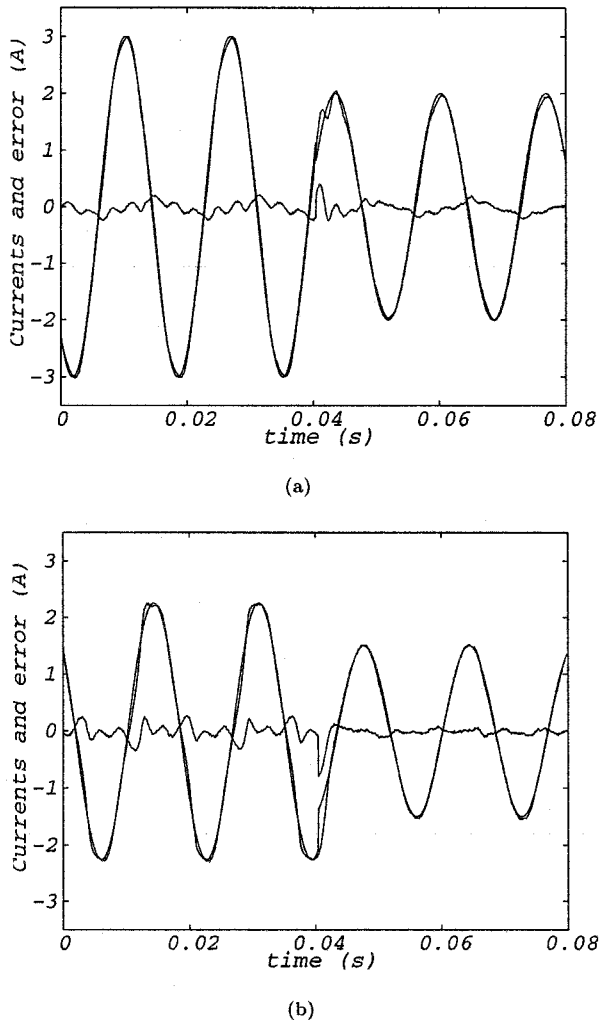

Fig. 10. Stator currents and current errors for the synchronous controller at 60 Hz. (a) d axis. (b) q axis.

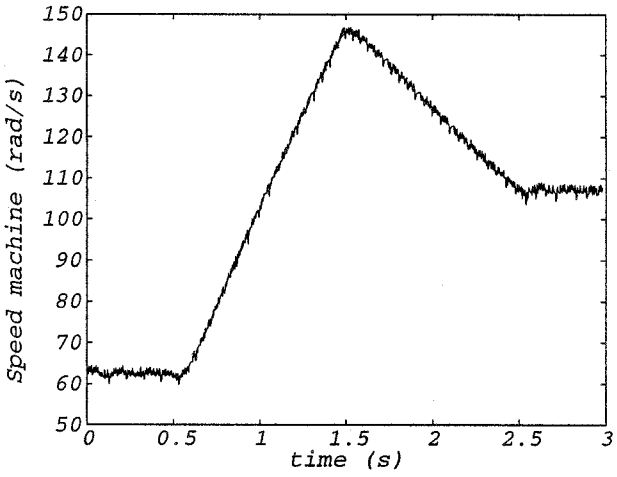

Fig. 11. Machine speed for the proposed field-oriented control scheme.

The results presented in Figs. 8–10 show that the current error increases when the frequency of the reference waveforms increases, particularly with the stationary controllers. Even at 60 Hz, the controller implemented by using synchronous reference frame coordinates provides acceptable performance, whereas the stationary one does not. The performance degradation seen for the stationary controller confirms the results in the simulation study.

Fig. 11 presents the machine speed when operating under field orientation with the current control being implemented in synchronous frame coordinates and without feedforward compensation. For these results, the reference amplitude of the rotor flux was kept constant and the reference torque was submitted to step changes similar to those used in the simulation test of Fig. 6. By observing the speed evolution, one can conclude that the torque control is satisfactory.

IX. Conclusion

The rotor-flux-oriented control of a single-phase motor was implemented and experimentally tested in the laboratory. It was shown that it is necessary to supply the main and auxiliary machine windings with unbalanced currents to eliminate the ac term of the electromagnetic torque. Furthermore, this unbalanced control is necessary to realize a balanced rotor-flux model which enables vector control to be applied to the single-phase motor.

The asymmetry of the single-phase machine also has an important impact on the design of the stator current control loop. The use of digital current controllers in both the stationary and synchronous reference frames has been investigated and has shown satisfactory closed-loop behavior, but, as expected, the synchronous controller provides the best performance at high frequency.

The proposed PWM technique was adapted from the standard space-vector modulation and is relatively simple to implement.

This paper has shown that is possible to implement high-performance ac drive systems with a single-phase motor for low-power applications. A prospective application of the proposed approach is its use as an emergency scheme for the drive system when a symmetric machine becomes asymmetric because of some winding failure.

References

[1] E. R. Collins Jr., A. B. Puttgen, and W. E. Sayle II, "Single-phase induction motor adjustable speed drive: Direct phase angle control of the auxiliary winding supply," in *Conf. Rec. IEEE-IAS Annu. Meeting*, 1988, pp. 246–252.

[2] M. F. Rahman and L. Zhong, "A current-forced reversible rectifier fed single-phase variable speed induction motor drive," in *Proc. IEEE PESC'90*, 1990, pp. 114–119.

[3] M. F. Rahman, L. Zhong, and S. Y. R. Hui, "A single-phase, regenerative, variable speed induction motor drive with sinusoidal input current," in *Proc. EPE Conf.*, 1995, pp. 3777–3780.

[4] D. G. Holmes and A. Kotsopoulos, "Variable speed control of single and two phase induction motors using a three phase voltage source inverter," in *Conf. Rec. IEEE-IAS Annu. Meeting*, 1993, pp. 613–620.

[5] C. C. Liu, C. M. Young, and C. H. Liu, "New inverter-driven design and control method for two-phase induction motor drives," *Proc. IEE—Elect. Power Applicat.*, vol. 143, no. 6, pp. 458–466, Nov. 1996.

[6] D. W. Novotny, T. A. Lettenmaier, and T. A. Lipo, "Single-phase induction motor with an electronically controlled capacitor," *IEEE Trans. Ind. Applicat.*, vol. 27, pp. 38–43, Jan./Feb. 1991.

[7] P. N. Enjeti and A. Rahman, "A new single-phase to three-phase converter with active input current shaping for low cost ac motor drives," in *Conf. Rec. IEEE-IAS Annu. Meeting*, 1990, pp. 935–939.

[8] P. C. Krause, O. Wasynczuk, and S. D. Sudhoff, *Analysis of Electric Machinery*. Piscataway, NJ: IEEE Press, 1995.
[9] H. Buhler, *Reglages Echantillonnes*, 1st ed. Lausanne, Switzerland: Presses Polytechnique Romandes-Dunod, 1983.
[10] M. P. Kazmierkowski and H. Tunia, *Automatic Control of Converter-Fed Drives*. Amsterdam, The Netherlands: Elsevier, 1994.

Maurício Beltrão de Rossiter Corrêa (S'97) was born in Maceió, Brazil, in 1973. He received the Bachelor's and Master's degrees in electrical engineering in 1996 and 1997, respectively, from the Federal University of Paraíba, Campina Grande, Brazil, where he is currently working toward the Doctoral degree.

Since 1997, he has also been a faculty member of the Escola Técnica Federal de Alagoas, Palmeira dos Indios, Brazil. His research interests include power electronics and electrical drives.

Cursino Brandão Jacobina (S'78–M'78–SM'98) was born in Correntes, Brazil, in 1955. He received the B.S. degree in electrical engineering from the Federal University of Paraíba, Campina Grande, Brazil, and the Diplôme d'Etudes Approfondies and the Ph.D. degree from the Institut National Polytechnique de Toulouse, Toulouse, France, in 1978, 1980, and 1983, respectively.

Since 1978, he has been with the Electrical Engineering Department, Federal University of Paraíba, where he is currently a Professor of Electrical Engineering. His research interests include electrical drives, power electronics, control systems, and system identification.

Antonio Marcus Nogueira Lima (S'77–M'89) was born in Recife, Brazil, in 1958. He received the B.S. and M.S. degrees in electrical engineering from the Federal University of Paraíba, Campina Grande, Brazil, and the Ph.D. degree from the Institut National Polytechnique de Toulouse, Toulouse, France, in 1982, 1985, and 1989, respectively.

He was with the Escola Técnica Redentorista, Campina Grande, Brazil, from 1977 to 1982 and was a Project Engineer with Sul-América Philips, Recife, Brazil, from 1982 to 1983. Since September 1983, he has been with the Electrical Engineering Department, Federal University of Paraíba, where he is currently a Professor of Electrical Engineering. His research interests are in the fields of electrical machines and drives, power electronics, electronic instrumentation, control systems, and system identification.

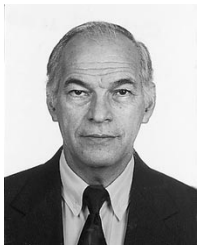

Edison Roberto Cabral da Silva (SM'95) was born in Pelotas, Brazil, in 1942. He received the B.C.E.E. degree from the Polytechnic School of Pernambuco, Recife, Brazil, the M.S.E.E. degree from the University of Rio de Janeiro, Rio de Janeiro, Brazil, and the D.Eng. degree from the University Paul Sabatier, Toulouse, France, in 1965, 1968, and 1972, respectively.

In 1967, he joined the staff of the Electrical Engineering Department, Federal University of Paraíba, Campina Grande, Brazil, where he is a Professor of Electrical Engineering and Director of the Research Laboratory on Industrial Electronics and Machine Drives. In 1990, he was with COPPE, Federal University of Rio de Janeiro, and from 1990 to 1991, he was with WEMPEC, University of Wisconsin, Madison, as a Visiting Professor. His current research work is in the areas of power electronics and motor drives. He was the General Chairman of the 1984 Joint Brazilian and Latin-American Conference on Automatic Control, sponsored by the Brazilian Automatic Control Society.

Dr. da Silva is currently a Member-at-Large of the Executive Board of the IEEE Industrial Applications Society.